Regression Analysis of Thermal Conductivity Based on Measurements of Compacted Graphite Irons

MARTIN SELIN and MATHIAS KÖNIG

A model describing the thermal conductivity of compacted graphite iron (CGI) was created based on the microstructure analysis and thermal conductivity measurements of 76 compacted graphite samples. The thermal conductivity was measured using a laser flash apparatus for seven temperatures ranging between 35 °C and 600 °C. The model was created by solving a linear regression model taking into account the influence of carbon and silicon additions, nodularity, and fractions of ferrite and carbide constituents. Observations and the results from the model indicated a positive influence of the fraction of ferrite in the metal matrix on the thermal conductivity. Increasing the amount of carbon addition while keeping the CE value constant, *i.e.*, at the same time reducing the silicon addition, had a positive effect on the thermal conductivity value. Nodularity is known to reduce the thermal conductivity and this was also confirmed. The fraction of carbides was low in the samples, making their influence slight. A comparison of the thermal conductivity values calculated from the model with measured values showed a good agreement, even on materials not used to solve the linear regression model.

I. INTRODUCTION

IN an engine, components such as cylinder blocks, cylinder heads, and piston rings are exposed to large variations in temperature that can give rise to thermal stresses and result in engine failure. The combination of strength and thermal transport properties of the engine material is therefore very important. Previous cast iron investigations have concluded that graphite morphology generally has the largest influence on the thermal conductivity.[1–3] Gray cast iron, with lamellar-shaped graphite, conducts heat more efficiently than compacted graphite iron (CGI) and the worst thermal properties are found in ductile cast iron, with nodular-shaped graphite. Gray cast iron has therefore been the material of choice in most engine components, due to its ability to remove heat rather than its strength. In the transport industry, there is an increasing demand for environmentally sustainable transport, driven by governmental decrees and customer requirements. Increasing an engine's peak firing pressure is one solution to meet these demands. With increasing engine temperatures, the combination of strength and thermal properties in gray cast iron are not good enough, due to poor strength at elevated temperatures. Attention is therefore directed toward CGI as a replacement material. Even though the thermal transport property is worse compared to gray cast iron, the improved strength justifies the change. The lower value of the thermal conductivity found in CGI

therefore requires further attention before a material with optimum properties can be achieved.

Various methods for approximation of the thermal conductivity in cast irons have previously been made by, for example, Helsing *et al.*[4,5] and Holmgren *et al.*[2,6] Helsing *et al.* used an average field approximation to derive models for the thermal conductivity value, while Holmgren *et al.* solved linear regression models. Thermal conductivity values for all three major graphite morphologies, *i.e.*, lamellar, compacted and nodular, could be calculated using any of the methods mentioned earlier. Both methods have advantages and disadvantages. The average field approximation is flexible and can be applied for a wide range of graphite shapes and microstructures. However, this method requires very accurate values of the thermal properties of the various microconstituents and sometimes rough approximations are needed. A regression model is based on the parameters believed to affect thermal conductivity significantly. These parameters are usually easy to measure and the model is based on experimental measurements, requiring no assumptions such as grain conductivities. One downside with this method is the large amount of data needed when solving the regression model. If the data set is too small or narrow, the model will not be as general and useful.

In models that include all graphite morphologies, there is a possibility that the parameter representing the morphology will dominate over other important parameters, due to the large influence on the thermal conductivity. By focusing on one morphology, the influence of other parameters will become more visible and will increase the accuracy of the calculated value.

The metal matrices in the cast iron samples investigated by Holmgren and co-workers had a predominately pearlitic metal matrix that could include free

MARTIN SELIN and MATHIAS KÖNIG, Postdoctoral Students, are with the Department of Mechanical Engineering, Materials and Manufacturing—Casting, Jönköping University, Jönköping, SE - 551 11, Sweden. Contact e-mail: martin.selin@jth.hj.se

cementite. In addition to these two microstructure constituents, ferrite is an important constituent when discussing thermal conductivity.[7] The aim of this work is to develop a temperature-dependent linear regression model that includes the fraction of ferrite as well as the fraction of carbide, the percent nodularity, and the additions of carbon and silicon. The last four parameters are included in the regression model by Holmgren et al.[6] The model will only be solved for CGI materials and for temperatures ranging between 35 °C and 600 °C. An accurate description of the temperature dependence is important because various microconstituents affect that dependence differently. In CGI materials, it is also common that the thermal conductivity value peaks at approximately 300 °C for some compositions, while being quite temperature independent for others. All of this is important for components operating at elevated temperatures. The data set for the model is based on microstructure analysis and thermal conductivity measurements of 76 CGI materials, and the key parameters were those considered as having the largest influence on the thermal conductivity value.

II. EXPERIMENTAL BACKGROUND

A. Material

The melts used in this experiment (Table I) were produced by using a medium-frequency induction melting furnace. The charges were made up of 1100 kg CGI returns, 700 kg ductile iron scrap, 700 kg ductile pig iron, 500 kg steel scrap, and an adjustment of carbon and alloying elements. Spheroidization and inoculation, using the sinter-cast method[8] and FeSi, respectively, were performed on approximately 500 kg of melt in a pouring ladle. Alloying elements were added to the base

iron to create five groups of CGI materials named Mg, Si, Cu, Sn, and Carb (Table I). The alloying additions used were FeSi, Cu, Sn, FeMn, FeCr, and FeMo. The FeMn was only added to the four last samples, i.e., Carb 1 through Carb 4, as a pearlite and carbide stabilizer. Optical emission spectroscopy equipment, ARL 3460 from Thermo Scientific, Waltham, MA, was used to determine the chemical composition.

The tapping and pouring temperature was approximately 1500 °C and 1350 °C, respectively, for all samples. Some melt was poured into furan sand molds to produce castings with shape and section diameters as shown in Figure 1(a); the rest of the melt was poured into a sampling cup, as illustrated in Figure 1(b). The cup has been developed and was previously used by Elmquist et al.[9] and was comprised of two geometries, one hemisphere and one cylindrical disk. The cup was made from sheet metal and the diameter of the disk was 70 mm. The cup was placed in a surrounding mold with three different thermal conductivities to produce three different cooling rates. The average cooling rates were 0.08, 0.2, and 0.7 K/s for slow, medium and fast cooling, respectively. The cooling rates were determined by the type N thermocouples, shown as black rods in Figure 1(b). The cooling rate for the castings cast in the
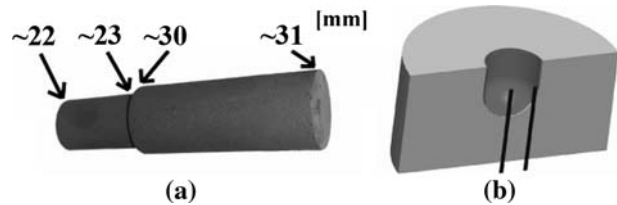

Fig. 1—Illustrations of (a) casting cast in furan sand mold and (b) sampling cup with surrounding mold.

Table I. Chemical Composition of Investigated Materials (Weight Percent)

Sample	C	Si	Mn	P	S	Cr	Ni	Mo	Cu	Sn	Mg	CEL**
Base iron	—*	2.10	<0.30	—	—	<0.05	<0.05	<0.05	0.60	0.05	—	—
Mg 1	3.63	2.11	0.31	0.016	0.007	0.03	0.01	0.01	0.66	0.040	0.006	4.17
Mg 2	3.57	2.14	0.31	0.017	0.007	0.03	0.02	0.01	0.67	0.041	0.013	4.11
Mg 3	3.45	2.13	0.32	0.017	0.007	0.03	0.02	0.01	0.68	0.041	0.020	3.99
Si 1	3.63	1.89	0.32	0.013	0.013	0.04	0.06	0.01	0.69	0.049	0.014	4.11
Si 2	3.54	2.31	0.32	0.014	0.013	0.04	0.06	0.01	0.67	0.049	0.015	4.12
Si 3	3.36	2.96	0.32	0.015	0.013	0.04	0.06	0.01	0.66	0.049	0.017	4.11
Si 4	3.19	3.85	0.32	0.016	0.012	0.05	0.06	0.01	0.64	0.049	0.016	4.16
Cu 1	3.53	2.01	0.31	0.015	0.009	0.05	0.03	0.01	0.26	0.048	0.011	4.04
Cu 2	3.43	2.07	0.30	0.015	0.009	0.05	0.03	0.01	0.51	0.048	0.011	3.96
Cu 3	3.54	2.09	0.30	0.015	0.008	0.05	0.03	0.01	0.84	0.047	0.010	4.07
Cu 4	3.63	2.07	0.29	0.014	0.009	0.06	0.03	0.01	1.31	0.047	0.012	4.15
Sn 1	3.60	2.06	0.32	0.029	0.010	0.04	0.04	0.01	0.61	0.015	0.015	4.13
Sn 2	3.64	2.08	0.32	0.029	0.010	0.04	0.04	0.01	0.62	0.032	0.014	4.17
Sn 3	3.67	2.09	0.32	0.029	0.010	0.04	0.04	0.01	0.62	0.060	0.013	4.21
Sn 4	3.58	2.02	0.32	0.029	0.011	0.04	0.04	0.01	0.61	0.095	0.014	4.10
Carb 1	3.61	2.30	0.60	0.016	0.008	0.04	0.02	0.01	0.59	0.052	0.012	4.19
Carb 2	3.61	2.29	0.60	0.015	0.008	0.10	0.02	0.01	0.59	0.051	0.012	4.19
Carb 3	3.60	2.29	0.60	0.014	0.008	0.15	0.02	0.01	0.59	0.052	0.010	4.18
Carb 4	3.56	2.29	0.60	0.018	0.009	0.15	0.02	0.10	0.59	0.052	0.012	4.14

*Amount of C was chosen so liquidus temperature became 1150 °C, $T_L = (14.743 - CE(\text{thermal}))/0.00895$.
**CE liquid value = C + Si/4 + P/2.

furan sand mold (Figure 1(a)) was not measured. The castings from the furan sand mold were denoted s.m. and the castings from the sampling cup were denoted s.c., and all were indexed 1, 2 and 3 for a fast, medium, and slow cooling rate, respectively.

Two adjacent cylindrical samples with a diameter and height of approximately 12.5 and 6.0 mm, respectively, were machined from the center of the thinner part of the castings in Figure 1(a). One sample was used for microstructure analysis and one for thermal diffusivity measurements. One cylindrical sample with a diameter and height of approximately 12.5 and 4.5 mm, respectively, was machined from the cup casting. This sample was taken from the hemisphere part just below the cylindrical disk. The thermal diffusivity was first measured on the sample, and then a microstructure analysis was made on the same sample.

B. Microstructure

Compacted graphite is usually classified according to ISO Standard 16112:2006 by a roundness shape factor, described by Eq. [1], Figure 2, and Table II, and the percent nodularity defined in Eq. [2].

$$\text{roundness shape factor} = \frac{A}{A_m} = \frac{4 \times A}{\pi \times l_m^2} \qquad [1]$$

where A is the area of the graphite particle, l_m is the maximum axis length of the particle, and A_m is the area of circle of diameter l_m.

$$\text{percent nodularity}$$
$$= \frac{\sum A_{\text{nodules}} + 0.5 \times \sum A_{\text{intermediates}}}{\sum A_{\text{all particles}}} \times 100 \qquad [2]$$
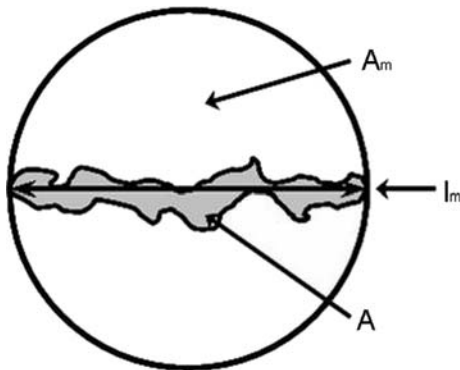

Fig. 2—Illustration of parameters used to define roundness shape factor.

Table II. Classification of Graphite Particle in CGI Materials

Roundness Shape Factor	Graphite Form
0.625 to 1	nodular (ISO form VI)
0.525 to 0.625	intermediate (ISO forms IV and V)
<0.525	compacted (ISO form III)

Note: Flake graphite particles and graphite particles with a maximum axis length less than 10 μm are not included in the analysis.

A Leitz DMRX optical microscope and Leica QWin Standard Y 2.8 image analysis software (Leica Microsystems, Wetzlar, Germany) were used for microstructure analysis and measurements. A total area of 27 and 10 mm^2 was analyzed for each s.c. and s.m. casting, respectively. Analysis of the unetched samples gave information about, for example, the percent nodularity and the graphite amount. In order to obtain information about the fractions of ferrite, pearlite, and carbide, the samples were etched with 2 pct Nital prior to analysis. In this experiment, the fraction sum of the graphite, ferrite, pearlite, and carbide constituents is 1.

C. Thermal Diffusivity

A Netzsch LFA 427 laser flash apparatus (Netzsch, Selb, Germany), illustrated in Figure 3, was used to investigate the thermal diffusivity D_T at seven temperatures ranging between 35 °C and 600 °C. At each investigated temperature, an average diffusivity value derived from five consecutive shots separated in time by 1 minute was used. This measurement technique is based on the principle developed by Parker et al.[10] This principle is that a short and intense laser pulse with a voltage of 450 V and a pulse width of 0.8 ms is absorbed at the front surface of the sample. An InSb infrared detector measured the temperature increase on the rear surface and the relative temperature increase was registered in a time-temperature diagram. The time needed for a 50 pct temperature increase was used when calculating the thermal diffusivity, and for adiabatic conditions the thermal diffusivity was calculated according to Eq. [3]:

$$D_T = \frac{0.1388 \times l^2}{t_{0.5}} \qquad [3]$$

where l was the sample thickness and $t_{0.5}$ was the time for a 50 pct temperature increase. Because measurements were not performed under adiabatic conditions,
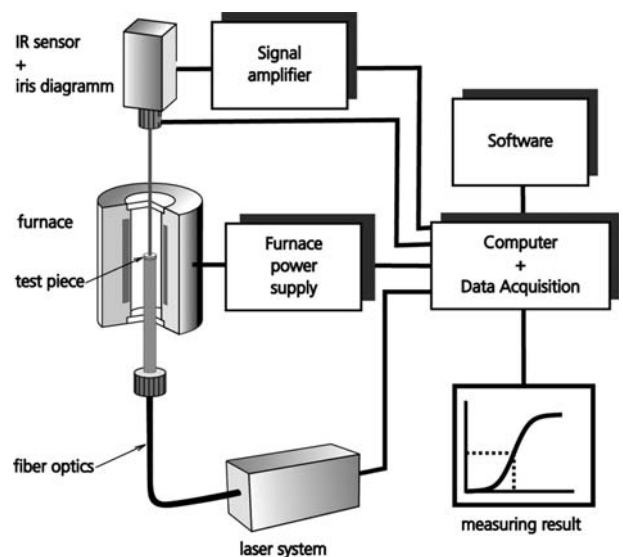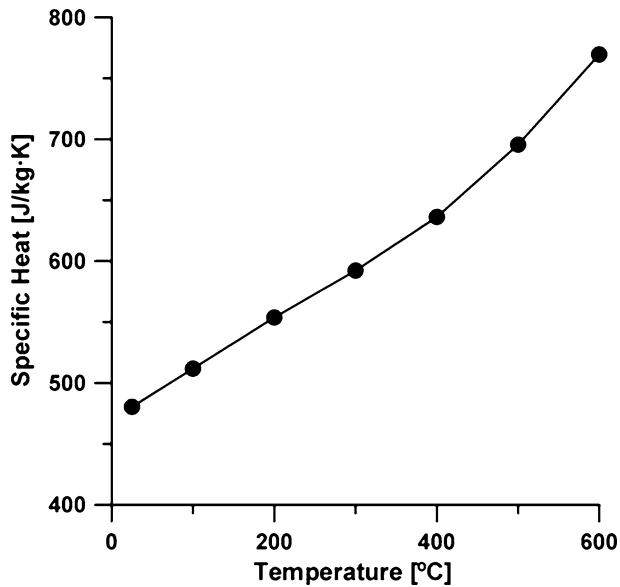

Fig. 3—Illustration of laser flash apparatus.

Fig. 4—Average specific heat values for various temperatures.[11]

Fig. 5—Illustration of deleterious effect of nodularity on thermal conductivity.

the software uses different mathematical models to consider the heat loss and laser pulse correction. A modified least square approximation, called a correlation coefficient, was used to find the most accurate approximation to the measured time-temperature curve. The thermal diffusivity value was calculated from the curve with the largest correlation coefficient value. The thermal conductivity λ was calculated from the thermal diffusivity, using Eq. [4]:

$$\lambda(T) = D_T(T) \times C_p(T) \times \rho(T) \qquad [4]$$

where C_p was the specific heat, ρ was the density, and T was the temperature in degrees Celsius. Values of specific heat have previously been measured using a Netzsch DSC 404 C Pegasus differential scanning calorimeter and the same average values, summarized in Figure 4, were used for these calculations.[11]

The density at room temperature ρ_{RT} was obtained by the Archimedes principle and the density at elevated temperature was obtained using Eq. [5]:

$$\rho(T) = \frac{\rho_{RT}}{(1 + \alpha \Delta T)^3} \qquad [5]$$

where ΔT was the temperature increase and α was the linear coefficient of thermal expansion. A Netzsch DIL 402 C dilatometer was used to measure the linear coefficient and an average value of $14.5 \cdot 10^{-6}$ K^{-1} was used in the calculations. The assumption of a small difference in C_p and α between various cast irons has previously been stated by Monroe and Bates.[12]

III. RESULTS AND DISCUSSION

A total of 76 CGI samples was measured and analyzed in this work. The samples could be divided into five groups, depending on which alloying element was varied (Table I). Due to the difference in chemical
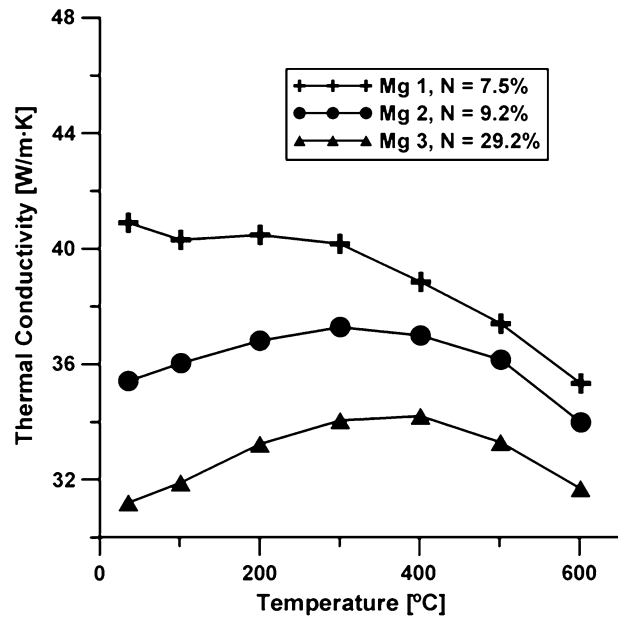
composition and cooling rate, microstructure parameters (for example, nodularity and fraction of ferrite) varied among all samples. The thermal conductivity and microstructure of the 19 CGI materials cast in the furan sand mold (Figure 1(a)) have previously been investigated and analyzed.

The negative influence of nodules on the thermal conductivity is well known[3,12,14] and could be illustrated by measurements on the samples with varying magnesium content, i.e., Mg 1, Mg 2, and Mg 3 cast in furan sand molds (Figure 5). From the figure it is evident that an increasing amount of nodular graphite particles decreased the thermal conductivity. The classification of CGI generally states that the nodularity should be less than 20 pct or, in some definitions, 30 pct in the material. By this definition, sample Mg 3 was no longer considered a CGI material. The same was true for all castings with a chemical composition according to Mg 3 (Table I).

The highly anisotropic properties of the graphite crystal structure, illustrated in Figure 6, together with the favorable growth direction of nodular graphite,[1,15,16] can explain the negative influence of nodularity on the thermal conductivity. The thermal conductivity value of graphite along the prism face is between 5 and 80 W/m·K, while the value along the basal plane is between 400 and 2000 W/m·K.[7] Nodular graphite grows in a radial manner along the c-axis and that, combined with the low thermal conductivity value along the prism phase, explains the poor thermal conductivity value for nodular-shaped graphite.

The large influence of carbon and silicon additions on thermal properties is shown in Figure 7. Keeping the carbon equivalent (CE) value constant while increasing the addition of silicon and decreasing the addition of carbon lowered the thermal conductivity. Graphite conducts heat very efficiently, implying that a reduction
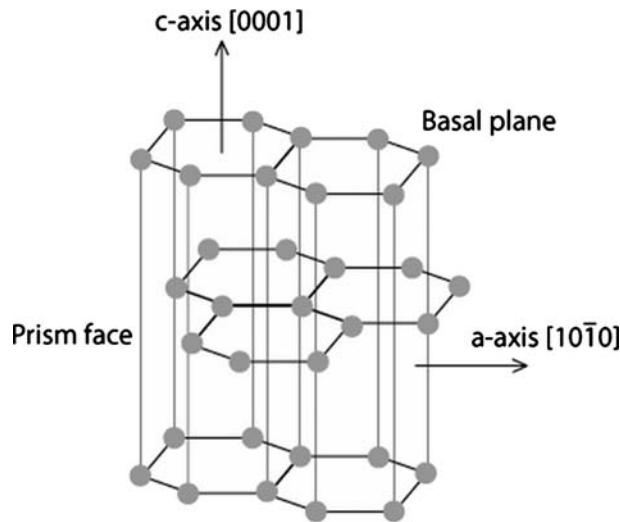
Fig. 6—Illustration of crystal structure of graphite.

Fig. 8—Influence of ferrite constituent on thermal conductivity of all CGI samples.
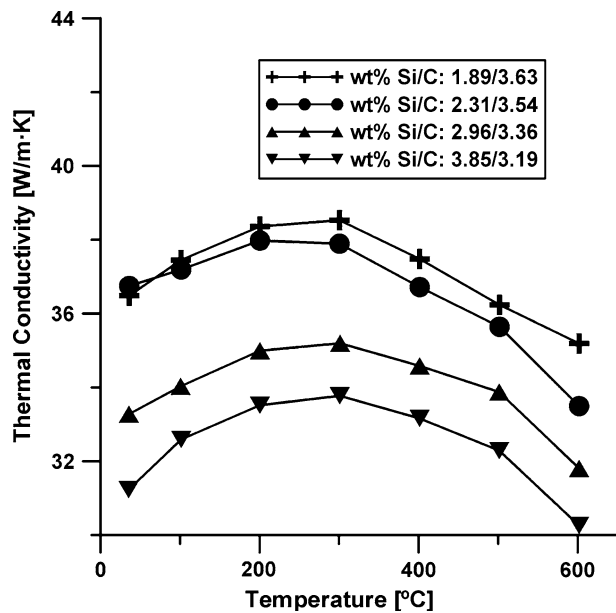

Fig. 7—Influence of silicon and carbon addition on thermal conductivity.

in graphite, *i.e.*, a lower addition of carbon, would reduce the thermal conductivity. Microstructure investigations showed, however, that the total area fraction of graphite was more or less unaffected among the samples. The change in chemical composition, between Si 1 and Si 4, resulted in an increase in the number of compacted graphite particles, while their average area was reduced. The explanation for that is the graphitizing property of silicon. However, this explanation alone does not explain the result in Figure 7.

Silicon is a ferrite-promoting element and, due to the known positive influence of ferrite,[7] increasing the addition of silicon should result in improved thermal conductivity. However, an exception to the positive
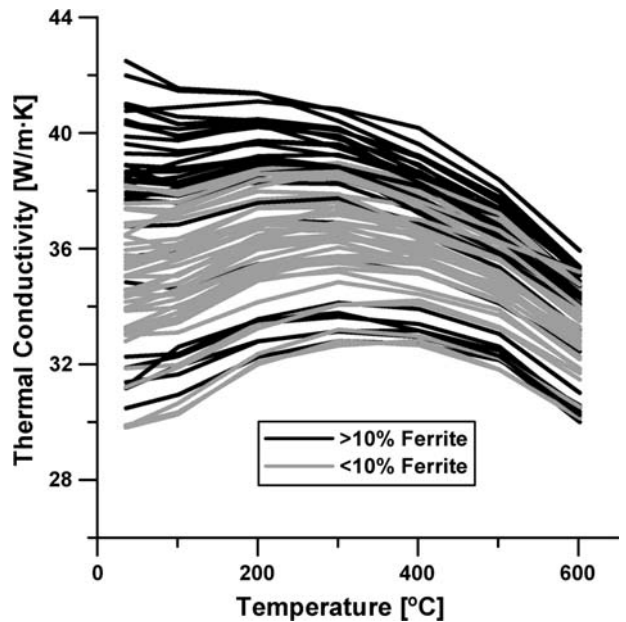
effect of ferrite on the thermal conductivity is ferrite with dissolved elements such as silicon that noticeably reduce the thermal conductivity in cast iron.[17] This explanation, together with the one mentioned earlier, explains the reduced thermal conductivity in Figure 7, with an increasing addition of silicon.

A confirmation of the positive influence of ferrite on the thermal conductivity is shown in Figure 8. The figure shows that large amounts of ferrite in the metal matrix generally increase the thermal conductivity, regardless of other microstructure features, such as, for example, nodularity. Figure 8 shows that although some samples contained a ferrite fraction larger than 10 pct, their thermal conductivity values were still among the lowest. Samples showing this behavior were those containing a large amount of silicon and a small amount of carbon, *i.e.*, samples Si 3 and Si 4. The reason for this is the same as discussed earlier. The fraction 10 pct was chosen because, below that amount, the ferrite did not completely surround the graphite particles, reducing the positive influence of the ferrite.

Ferrite has a thermal conductivity value close to the value for pure iron: approximately 80 W/m·K. Cementite, on the other hand, has very poor thermal properties, with a conductivity value of approximately 8 W/m·K. Such a difference in value can be explained by the movement of free electrons, which is the main transport mechanism of heat in metals.[18] Impurities, lattice mismatches, *e.g.*, grain boundaries, and a less favorable lattice structure will reduce the movement of the free electrons and diminish the thermal properties of a medium. In the comparison between ferrite and cementite (or carbides), the bcc structure of ferrite with very little dissolved carbon is more favorable than the orthogonal lattice found in cementite. Pearlite consists of alternating layers of cementite and ferrite, which also
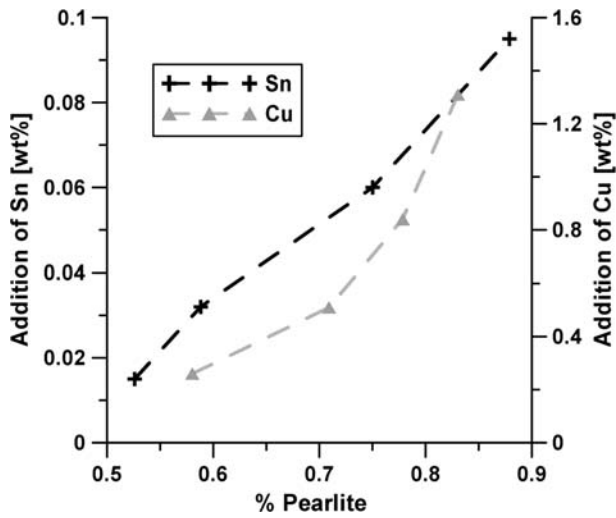
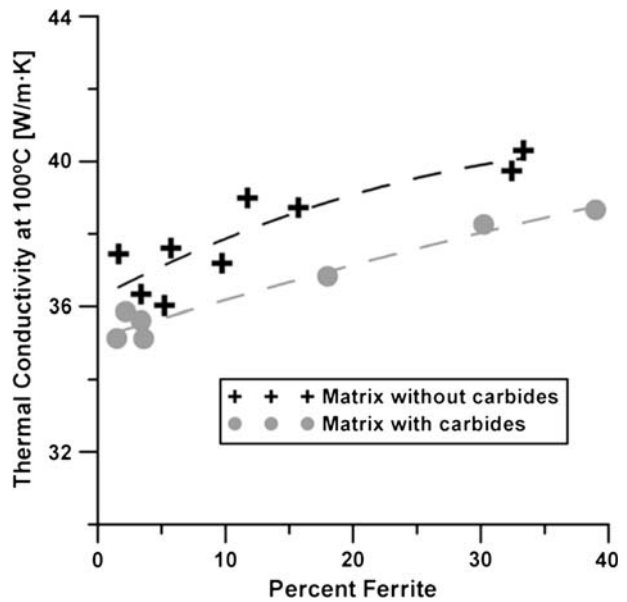Fig. 9—Illustration of pearlite-promoting effects of tin and copper.

Fig. 11—Influence of carbide constituent on thermal conductivity of CGI samples cast in furan sand mold.[13]
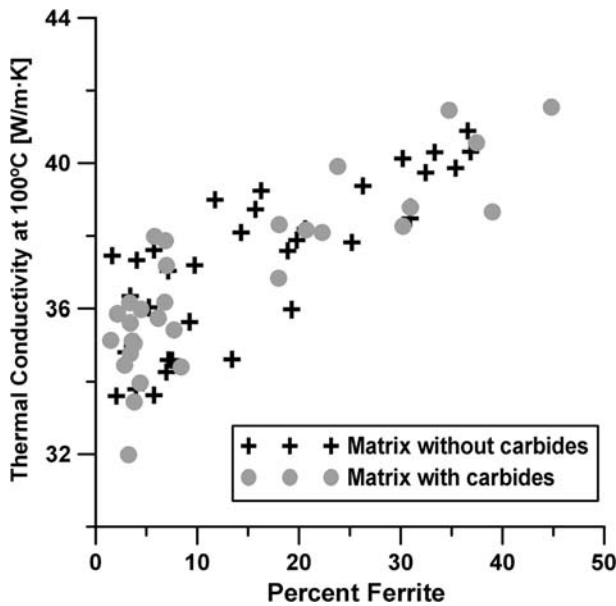

Fig. 10—Influence of carbide constituent on thermal conductivity of all CGI samples.

has a negative influence on the movement of the free electrons. A general thermal conductivity value of pearlite is therefore approximately 25 W/m·K. Copper and tin are both pearlite-promoting elements, as illustrated in Figure 9 for s.m. castings Cu 1 through Cu 4 and Sn 1 through Sn 4. Increasing additions of those elements, therefore, reduced the thermal conductivity.

To investigate the deleterious effect of carbides, the CGI samples were divided into two groups: one with a fraction of more than 0.1 pct carbides and one with fewer or no carbides. The influence of carbide was investigated by comparing the influence of the fraction of ferrite and the thermal conductivity value at 100 °C for the two groups (Figure 10). In that comparison, values associated with samples Mg 3, Si 3, and Si 4 are

not included, to more clearly illustrate the effect of the carbide constituent. As discussed earlier, castings with a chemical composition according to Mg 3 had a very high nodularity and a large addition of silicon promoted unfavorable ferrite; therefore, these samples were not representative of a typical CGI material.

If carbides have a deleterious effect on the thermal conductivity, the samples containing carbides should have a lower value compared to the carbide-free samples for a specific ferrite fraction. That effect is not possible to see in Figure 10, which shows that an increasing fraction of ferrite increases the thermal conductivity value. The fraction of carbides in all samples was very low, with a maximum fraction of 1.1 pct. However, the castings from the furan sand mold generally contained a larger fraction of carbides, compared to castings cast in the sampling cup. In the sampling cup, the carbide fraction ranged between 0.1 and 0.5 pct, while in the other samples, it ranged between 0.4 and 1.1 pct. If the same comparison was made with just the s.m. castings, a slight trend was possible to see (Figure 11). Even though the trend was slight, it showed that for a specific fraction of ferrite, the thermal conductivity value was lower for the samples containing carbides. It seemed likely that the fraction of carbides had to reach a certain threshold value before it affected the thermal conductivity, but the small variation in the conductivity values made the comparison harder.

The variation in cooling rate affected the nodularity and fraction of ferrite, illustrated in Figure 12 by samples Sn 1 and Sn 2. A comparison between the samples cast in the sampling cup gave some indications of how the cooling rate affected these parameters. The nodularity was higher in the fast cooling samples, due to more nucleation points and less time for carbon diffusion. The fraction of ferrite was generally higher for a chemical composition cooled with the medium
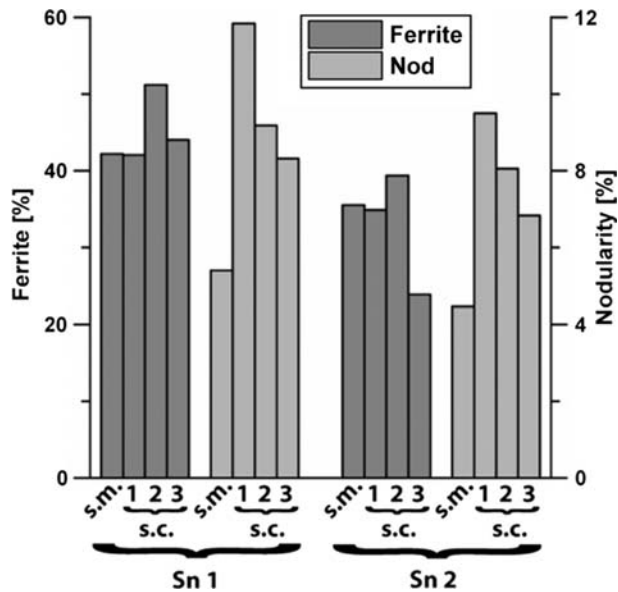
Fig. 12—Illustration of how cooling rates influence fraction of ferrite and nodularity.
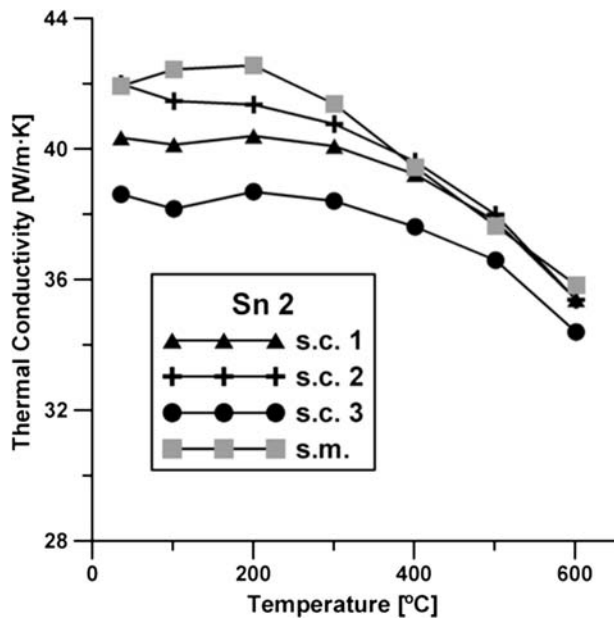

Fig. 13—Illustration of influence of cooling rate on thermal conductivity.

Table III. Summary of Five Key Parameters That Have a Large Influence on Thermal Conductivity

Parameters	Maximum	Minimum	Average
Carbon (wt pct)	3.67	3.19	3.55
Silicon (wt pct)	3.85	1.89	2.27
Nodularity (pct)	33.8	2.4	10.3
Ferrite (pct)	71.9	1.5	17.0
Carbide (pct)	1.1	0.0	0.1

Table IV. Summary of Temperature-Dependent β Constants after Solving Linear Regression Model

T (°C)	β_0	β_1	β_2	β_3	β_4	β_5
35	34.60	3.96	−5.22	−0.25	−2.94	0.12
100	33.27	3.96	−4.58	−0.23	−2.59	0.11
200	33.86	3.67	−3.99	−0.20	−2.20	0.09
300	35.23	3.05	−3.55	−0.17	−2.08	0.07
400	35.22	2.58	−3.12	−0.14	−2.02	0.06
500	34.94	2.07	−2.63	−0.13	−1.98	0.04
600	30.71	2.44	−2.26	−0.12	−1.47	0.03
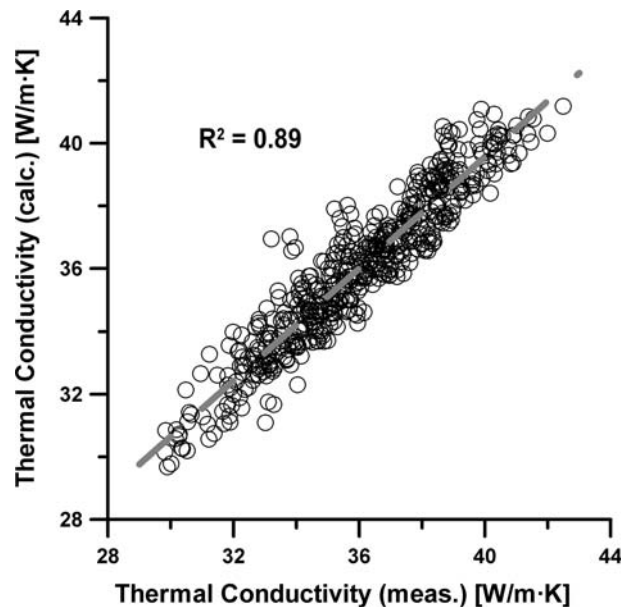
Fig. 14—Comparison of agreement between measured and calculated thermal conductivity values.

cooling rate compared with the other two cooling rates. Comparing the nodularity between castings from the furan sand mold and castings from the sampling cup seemed to indicate that the cooling rate in the furan sand mold was the slowest of the four.

The influence of cooling rate on the thermal conductivity was quite complex. A fast cooling rate increased nodularity, which had a deleterious effect on the thermal conductivity. However, at the same time, the fraction of ferrite increased, which had a positive influence. The variation in thermal conductivity values for a specific chemical composition was quite small, as illustrated in

Figure 13 by Sn 2, but the trends discussed later in this article were found for almost all compositions. The samples cast in the sampling cup with the medium cooling rate, i.e., s.c. 2, generally had a higher thermal conductivity value compared to the other two cooling rates (Figure 13). The reason for that was thought to be the larger fraction of ferrite and the decreased nodularity. Compared to the s.m. castings, the sampling cup samples had a lower thermal conductivity, probably due to a higher nodularity.

Based on the results discussed earlier, it was concluded that the parameters most affecting the thermal conductivity were the amounts of ferrite and carbide,

the additions of carbon and silicon, and the nodularity. The influence of the cooling rate was taken into account, as already mentioned. Table III summarizes the maximum, minimum, and average values of these five parameters for the 76 investigated CGI materials, to illustrate the range over which the parameters varied.

Based on the parameters summarized in Table III, a linear regression model was solved to find an approximate value of the thermal conductivity (Eq. [6]):

$$\lambda(T) = \beta_0(T) + \beta_1(T) \times C + \beta_2(T) \times Si + \beta_3(T) \\ \times Nod + \beta_4(T) \times f_{Fe3C} + \beta_5(T) \times f_\alpha \quad [6]$$

The temperature-dependent β constants were determined for the 76 CGI materials at the seven measured temperatures, and their units are consistent with those in Table III. The constants are summarized in Table IV at each temperature. By interpolation, β constants for any temperature could easily be derived.

To check that the solution was acceptable, the same data set of parameters used to solve the regression model were used together with the β constants to calculate thermal conductivity values. The calculated values were then compared with the measured values to confirm an acceptable agreement, and the results are summarized in Figure 14.

Analyzing the β constants showed that the constants affecting the contribution of carbon and ferrite, i.e., β_1 and β_5, are positive, while β_2, β_3, and β_4 are negative (Table IV). That confirmed the positive influence of graphite and large amounts of ferrite on the thermal conductivity and the negative influence of large amounts of silicon, nodularity, and carbides. The same trends of a negative influence of nodularity and carbides were also seen in References 2 and 6. Compared to Reference 6, some differences were seen in the sign of the constant related to silicon and the temperature dependence of carbide, but no further investigation of that difference was made in this work. All constants showed a temperature dependence, and all constants except β_0 tended toward zero, indicating a reduced influence of the parameters on the thermal conductivity with increasing temperature.

To more clearly see the influence of the key parameters on the calculated thermal conductivity values, the β constants were recalculated based on the normalized

Table V.   Summary of Recalculated β Constants after Solving the Linear Regression Model Using Normalized Values

T (°C)	β_0	β_1	β_2	β_3	β_4	β_5
35	34.60	14.03	−11.84	−2.53	−0.30	2.13
100	33.27	14.04	−10.37	−2.33	−0.27	1.89
200	33.86	13.03	−9.03	−2.02	−0.23	1.51
300	35.23	10.80	−8.03	−1.76	−0.21	1.19
400	35.22	9.14	−7.08	−1.43	−0.21	0.97
500	34.94	7.33	−5.95	−1.36	−0.20	0.72
600	30.71	8.66	−5.12	−1.20	−0.15	0.52

Table VI.   Values of Five Key Parameters from Holmgren et al.[6] Used to Test Equation [6]

Sample	Carbon (Wt Pct)	Silicon (Wt Pct)	Nodularity (Pct)	Carbide (Pct)	Ferrite (Pct)
Holmgren 1	3.56	2.12	20.2	1.7	0
Holmgren 2	3.56	2.12	28.9	trace*	0
Holmgren 3	3.54	2.12	19.7	3.1	0
Holmgren 4	3.54	2.12	30.1	trace*	0

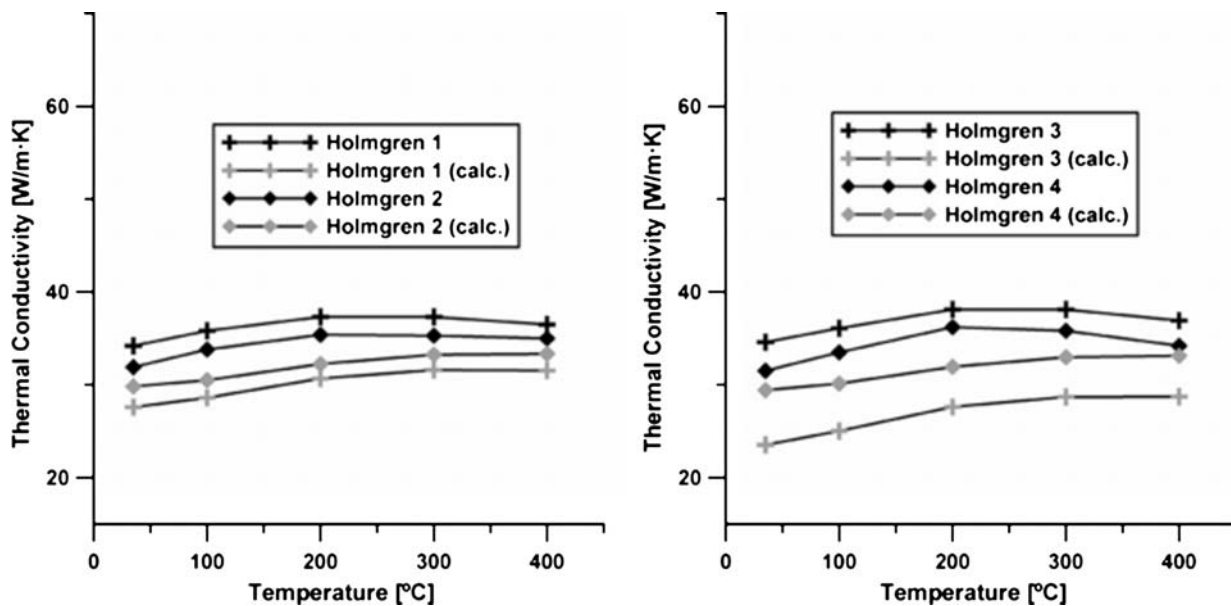*In the equation, a value of 0.2 pct was used as an approximate value.

Fig. 15—Comparison of calculated thermal conductivity values using regression equation, with measured thermal conductivity values by Holmgren et al.[6]

Example	Carbon (Wt Pct)	Silicon (Wt Pct)	Nodularity (Pct)	Carbide (Pct)	Ferrite* (Pct)
Dawson 1	3.48	2.12	2	0	4.5 (5)
Dawson 2	3.49	2.18	27	0	1.8 (2)
Dawson 3	3.66	2.26	3	0	1.8 (2)
Dawson 4	3.74	2.35	30	0	0 (0)
Dawson 5	3.57	2.10	5	0	18 (20)
Dawson 6	3.58	2.15	19	0	18 (20)
Dawson 7	3.73	2.35	10	0	27 (30)

*In Ref. 19, the fraction sum of ferrite and pearlite was 1. The numbers in brackets are values from Ref. 19; the others are recalculated fractions of ferrite, assuming a graphite content of 10 pct.

values of the key parameters. The normalization was made by dividing the actual values with their mean values, and the recalculated constants are summarized in Table V.

The recalculated β constants showed a very large influence of carbon and silicon addition on the thermal conductivity value and a fairly large influence of nodularity and fraction of ferrite. The influence of carbides was small, according to Table V, but the influence increased at higher temperatures. The low influence of the carbides is consistent with the results summarized in Figure 10.

Holmgren et al.[6] and Dawson[19] have previously made thermal conductivity measurements on various CGI materials. To further investigate the validity of the
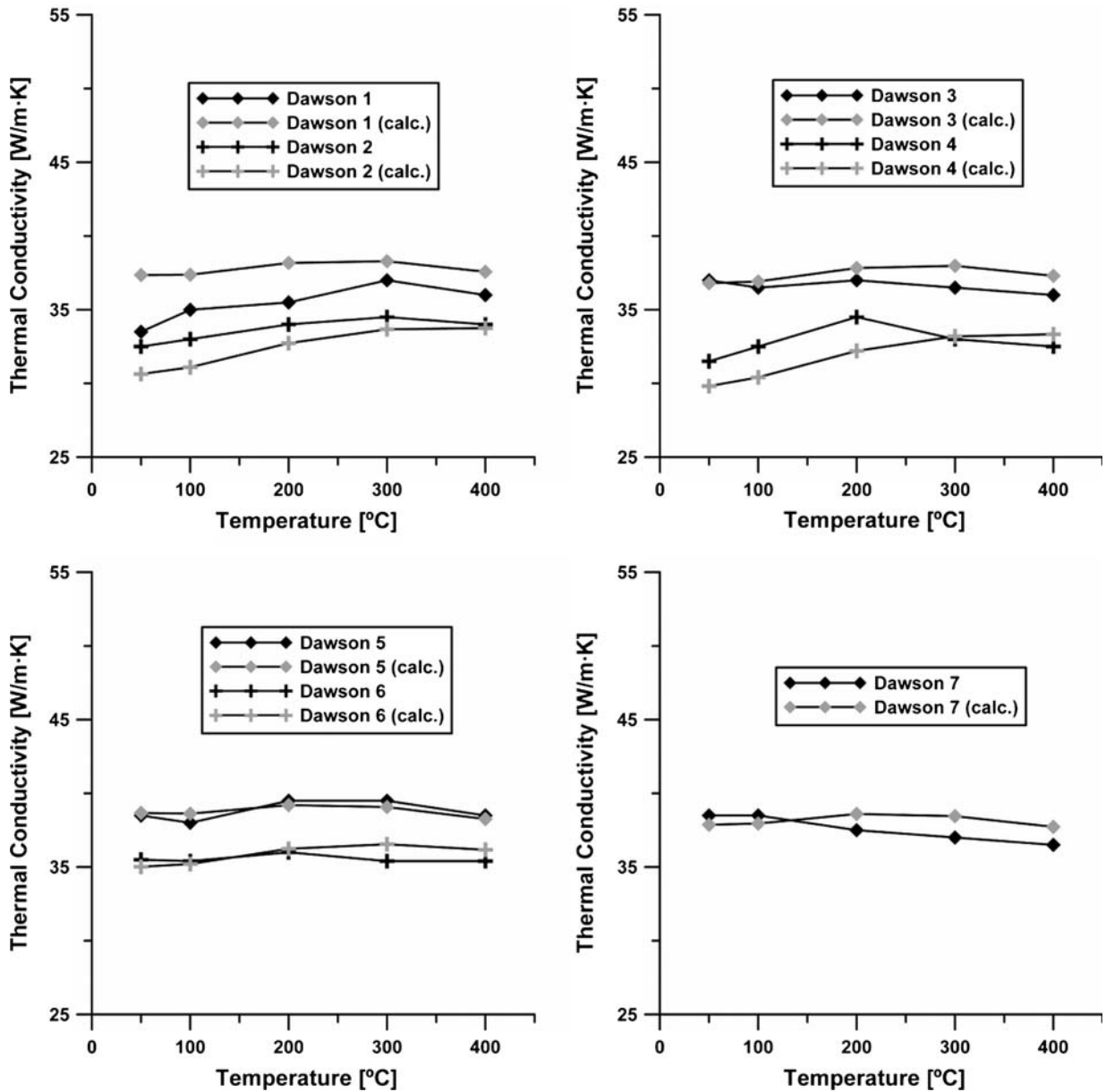

Fig. 16—Comparison of calculated thermal conductivity values using regression equation, with measured thermal conductivity values by Dawson.[19]

regression model (Eq. [6]), parameter values from these authors were inserted in the equation and the thermal conductivity was calculated.

The values of the five key parameters from Reference 6 are summarized in Table VI and the comparison between the measured thermal conductivity values and the calculated thermal conductivity values are plotted together in Figure 15. The index "calc." represents the value obtained from the regression equation when inserting values of the key parameters for that specific sample, *i.e.*, Holmgren 1 (calc.) indicated that values of key parameters from Holmgren 1 were inserted in Eq. [6].

Table VII summarized the parameters from Reference 19, and Figure 16 summarized the comparison of the thermal conductivity values.

There is a good agreement between the measured values of thermal conductivity and those calculated by the model, provided that the values of parameters do not differ drastically from those used to derive the regression model formula. The large differences in the values of the parameter explain the poor agreement observed for the Holmgren cases 1 and 3, with larger nodularity and carbide fraction. If these cases are excluded, the difference between the calculated and measured thermal conductivity was rather small and in samples Dawson 3, 5, 6, and 7, the values were almost identical. These comparisons confirmed that the derived equation could be used to approximate thermal conductivity values with good accuracy for temperatures ranging between 35 °C and 600 °C.

IV. CONCLUSIONS

A linear regression model describing the thermal conductivity of CGI for temperatures between 35 °C and 600 °C was generated based on measurements of microstructure parameters and thermal conductivity values of 76 CGI samples. The materials had 19 different chemical compositions and four different cooling rates for each composition, resulting in a wide range of microstructural constituents. The parameters included in the model were additions of carbon and silicon, nodularity, and fractions of ferrite and carbide. Based on microstructure analyses and thermal conductivity measurements, it can be concluded that these five parameters have the strongest influence on thermal conductivity. A comparison between the measured and calculated values of thermal conductivity shows a good agreement if the parameters do not differ radically from those used in the derivation of the regression formula.

REFERENCES

1. D. Holmgren, R. Källbom, and I.L. Svensson: *Metall. Mater. Trans. A*, 2007, vol. 38A, pp. 268–75.
2. D. Holmgren, A. Diószegi, and I.L. Svensson: *Int. J. Cast Met. Res.*, 2007, vol. 20 (1), pp. 30–40.
3. D.M. Holmgren, A. Diószegi, and I.L. Svensson: *Int. J. Cast Met. Res.*, 2006, vol. 19 (6), pp. 303–13.
4. J. Helsing and G. Grimvall: *J. Appl. Phys.*, 1991, vol. 70 (3), pp. 1198–1206.
5. J. Helsing and A. Helte: *J. Appl. Phys.*, 1991, vol. 69 (6), pp. 3583–88.
6. D. Holmgren and M. Selin: *5th Int. Conf. on Solidification and Gravity*, Miskolc-Lillafüred, Hungary, 2008, p. 6.
7. D. Holmgren: *Int. J. Cast Met. Res.*, 2005, vol. 18 (6), pp. 331–45.
8. W. Guesser, T. Schroeder, and S. Dawson: *Trans. Am. Foundry Society and the 105th Annual Castings Congr.*, Dallas, TX, American Foundry Society, Des Plains, IL, 2001, pp. 1–11.
9. L. Elmquist: Doctoral Thesis, Chalmers University of Technology, Göteborg, Sweden, 2009.
10. W.J. Parker, R.J. Jenkins, C.P. Butler, and G.L. Abbott: *J. Appl. Phys.*, 1961, vol. 32 (9), pp. 1679–84.
11. D. Holmgren, A. Diószegi, and I.L. Svensson: *Tsinghua Sci. Technol.*, 2008, vol. 13 (2), pp. 80–85.
12. R.W. Monroe and C.E. Bates: *Transactions of the American Foundrymen's Society, Proceedings of the 86th Annual Meeting*, Chicago, IL, 1982, pp. 615–24.
13. M. Selin, D. Holmgren, and I.L. Svensson: *Int. J. Cast Met. Res.*, 2009, vol. 22 (1–4), pp. 283–85.
14. W. Shenqing: *Trans. Jpn. Foundrymen's Soc.*, 1994, vol. 13, pp. 13–17.
15. P.C. Liu and C.R. Loper, Jr.: *Scanning Electron Microscopy*, 1980, pp. 407–18.
16. S.V. Subramanian, D.A.R. Kay, and G.R. Purdy: *Transactions of the American Foundrymen's Society, Proceedings of the 86th Annual Meeting*, Chicago, IL, 1982, pp. 589–603.
17. M.C. Rukadikar and G.P. Reddy: *J. Mater. Sci.*, 1986, vol. 21 (12), pp. 4403–10.
18. P.G. Klemens and R.K. Williams: *Int. Met. Rev.*, 1986, vol. 31 (5), pp. 197–215.
19. S. Dawson: *VDI Berichte, VDI Conference on Materials in Powertrain*, Dresden, Germany, October 28–29, 1999, No. 1472, pp. 85–105.